Physical, Spectroscopic, and Biological Properties of Ruthenium and Osmium Photosensitizers Bearing Diversely Substituted 4,4'-di(styryl)-2,2'-bipyridine Ligands

Robin Vinck, Johannes Karges, Mickaël Tharaud, Kevin Cariou, Gilles Gasser

▶ **To cite this version:**

Robin Vinck, Johannes Karges, Mickaël Tharaud, Kevin Cariou, Gilles Gasser. Physical, Spectroscopic, and Biological Properties of Ruthenium and Osmium Photosensitizers Bearing Diversely Substituted 4,4'-di(styryl)-2,2'-bipyridine Ligands. Dalton Transactions, 2021, 10.1039/D1DT02083H . hal-03351248

HAL Id: hal-03351248
https://hal.science/hal-03351248

Submitted on 22 Sep 2021

HAL is a multi-disciplinary open access archive for the deposit and dissemination of scientific research documents, whether they are published or not. The documents may come from teaching and research institutions in France or abroad, or from public or private research centers.

L'archive ouverte pluridisciplinaire **HAL**, est destinée au dépôt et à la diffusion de documents scientifiques de niveau recherche, publiés ou non, émanant des établissements d'enseignement et de recherche français ou étrangers, des laboratoires publics ou privés.

Physical, Spectroscopic, and Biological Properties of Ruthenium and Osmium Photosensitizers Bearing Diversely Substituted 4,4'-di(styryl)-2,2'-bipyridine Ligands

Robin Vinck,[a] Johannes Karges,[a] Mickaël Tharaud,[b] Kevin Cariou,[a] and Gilles Gasser[a,]*

[a] Chimie ParisTech, PSL University, CNRS, Institute of Chemistry for Life and Health Sciences, Laboratory for Inorganic Chemical Biology, 75005 Paris, France.

[b] Institut de Physique du Globe de Paris, Biogéochimie à l'Anthropocène des Eléments et Contaminants Emergents, 75005 Paris, France.

* Corresponding authors: gilles.gasser@chimieparistech.psl.eu; www.gassergroup.com; Tel. +33 1 44 27 56 02.

ORCID-ID:

Robin Vinck: 0000-0002-2730-0121

Johannes Karges: 0000-0001-5258-0260

Mickaël Tharaud: 0000-0001-6131-655X

Kevin Cariou: 0000-0002-5854-9632

Gilles Gasser: 0000-0002-4244-5097

Keywords:

Bioinorganic chemistry; Medicinal Inorganic Chemistry; Photodynamic therapy; Ruthenium complexes; Structure-Activity Relationship.

ABSTRACT

Capitalising on the previous identification of a distyryl coordinated Ru(II) polypyridine complex as a promising photosensitizer for photodynamic therapy, eight new complexes were synthesized by modifications of the ligands or by changing the metal coordinated. We report in this work the effects of these modifications on the physical, spectroscopic, and biological properties of the synthesized complexes. Subtle structural modifications of the distyryl ligand only had a moderate effect on the corresponding complexes visible light absorption and singlet oxygen quantum yield. These modifications however had a significant effect on the

lipophilicity, the cellular uptake and the phototoxicity of the complexes. Although the lipophilicity of the complexes had a somewhat expected effect on their cellular uptake, this last parameter could not be directly correlated to their phototoxicity, revealing other underlying phenomena. Overall, this work allowed to identify two promising ruthenium complexes as photosensitisers for photodynamic therapy and provides some guidance on how to design better photosensitizers.

INTRODUCTION

As an alternative to conventional cancer treatments, photodynamic therapy (PDT) has become an intensively investigated field of study these past decades.[1] In particular, the development of new photosensitizer (PS), able to efficiently harvest the energy from light irradiation to generate oxidative damages to the targeted tissues is an everlasting challenge.[2] Although the first studied PSs were purely organic molecules, our group and others have focused on the development of metal-containing PSs, such as ruthenium (Ru) polypyridyl complexes. These metal complexes are ideal candidates due to their attractive photophysical and biological properties (*i.e.*, high water solubility, high biocompatibility, high chemical stability, high production of reactive oxygen species, large Stokes shift).[3–11]

We recently described a series of Ru(II) polypyridyl complexes bearing a 4,4'-di(styryl)-2,2'-bipyridine ligand as efficient 1- and 2-photon PSs (Fig. 1) and their encapsulation into polymers for selective delivery.[12–14] These PSs were rationally designed to generate compounds with a bathochromic absorption shift by π-extension of the ligand scaffold and functionalisation with electron donor substituents of the respective Ru(II) polypyridine complexes. This is a desired property as longer wavelengths penetrate deeper in the tissues, allowing to potentially target deeply implanted tumours.

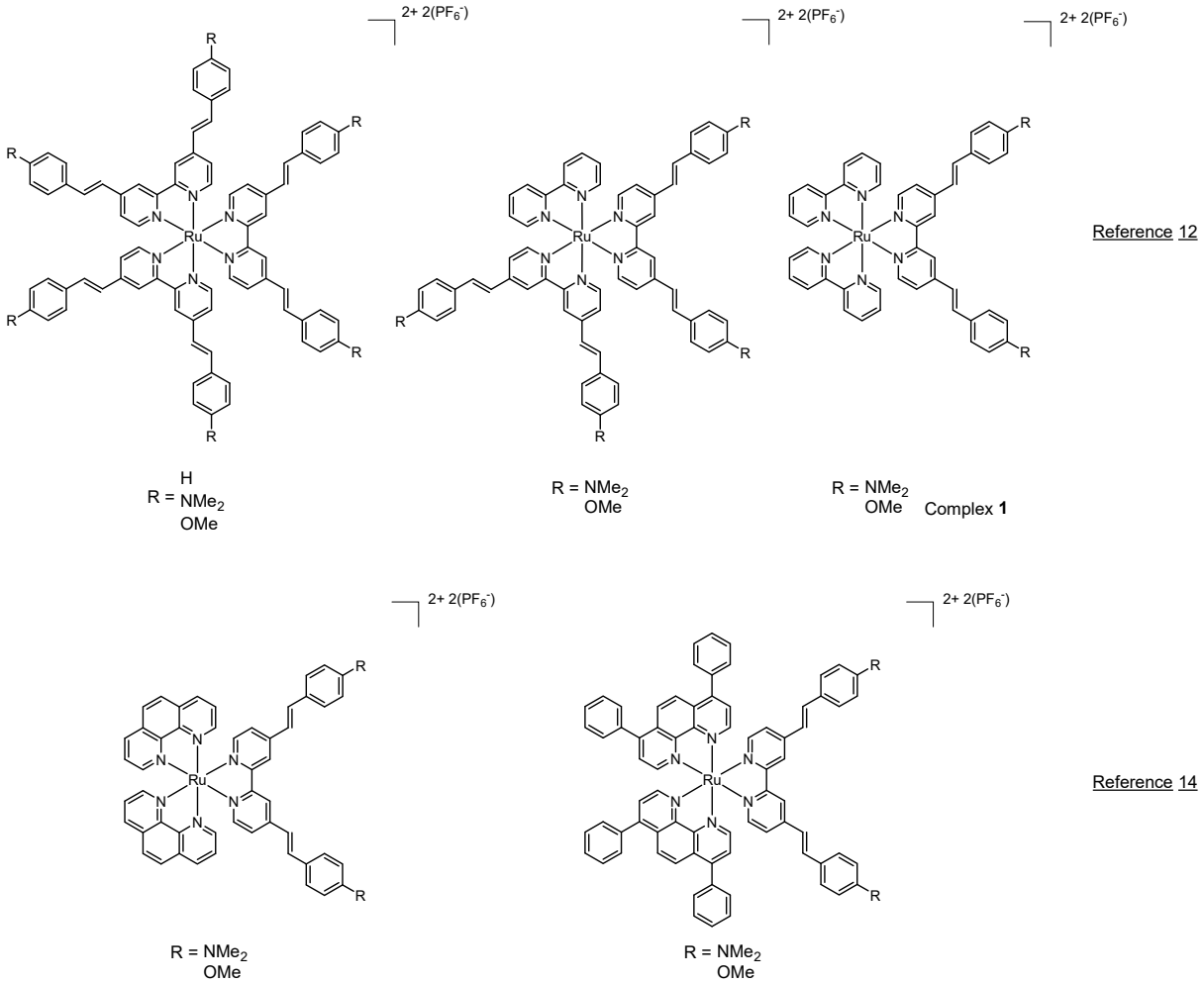

Figure 1. Molecular structures of some of the previously studied distyryl ligand-based Ru PSs.[12,14]

Although this strategy yielded efficient PSs with an absorption tail near the biological spectral window (600-900 nm), other properties need to be considered from a drug development point of view, such as solubility, cellular uptake and, eventually, photodynamic efficiency. These properties can be drastically affected by the nature of a single substituent, as we recently reported in the case of $Ru(dppz)_3$ complexes.[15] In this work, we report the results of a structure-activity relationship (SAR) study based on the structure of complex **1**.[12]

RESULTS AND DISCUSSION

Scope

In this work, a SAR study of complex **1**, which showed the strongest therapeutic effect during previous investigations,[12] was attempted in order to further improve its therapeutic efficiency (Fig. 2). Eight complexes were synthesized, by varying the position of the methoxy substituent on the distyryl ligand's phenyl ring (complexes **2** and **3**) or the nature of this substituent, using electron-donating or -withdrawing groups (complexes **4**-**7**). Complex **8** was obtained by exchanging the two 2,2'-bipyridine ligands with two 2,2'-bipyrazine ligands in an attempt to increase the aqueous solubility of the complex. Finally, complex **9** was obtained by replacing

the Ru metallic centre with osmium, as coordinatively saturated osmium complexes have demonstrated a great PDT potential owing to their increased photostability and higher absorption wavelengths.[16–22]

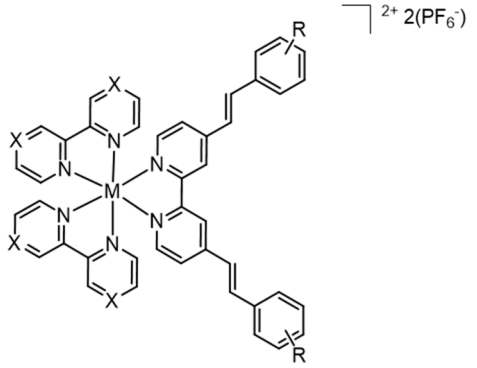

M	X	R	#
Ru	CH	p-OMe	1
		m-OMe	2
		o-OMe	3
		p-OH	4
		p-NH_2	5
		p-F	6
		p-NO_2	7
	N	p-OMe	8
Os	CH		9

Figure 2. Molecular structures of the evaluated complexes. The complexes were isolated as PF_6^- salts and used as racemic mixtures.

Synthesis and Characterization

The synthetic strategy for the synthesis of the desired Ru(II) polypyridine complexes is outlined in Scheme S1. The hydroxy and nitro functionalised ligands were synthesised according to previously published procedures.[23] The methoxy or fluoro substituted distyryl ligands were prepared from 4,4´-dimethyl-2,2´-bipyridine and the respective benzaldehyde in the presence of potassium *tert*-butoxide. Attempts to synthesise the amine functionalised distyryl ligand analogously were unsuccessful. The synthetic strategy was therefore changed, and this ligand was prepared from a sodium dithionite-mediated reduction of the nitro ligand. With these ligands in hand, the desired Ru(II) polypyridine complexes were synthesised. Ru(III) chloride was reduced to Ru(II) with ethanol. Upon addition of two equivalents of the nitrogen donating bidentate ligand (2,2´-bipyridine or bipyrazine) and an excess of lithium chloride, the dichloro biscoordinated Ru(II) polypyridine complexes were prepared. Finally, the chloride ligands were substituted with the previously prepared distyryl ligand and the desired metal complexes formed. All complexes were characterized by ^1H and ^{13}C NMR (Fig. S1-S14) and HRMS (Fig. S15-S21) and their purity was confirmed by elemental analysis. Of note, complex **5** has already been described previously, but to the best of our knowledge has never been evaluated as a PDT PS.[24]

UV-Vis Absorption

To better understand the individual effect of each modification on the photophysical properties of the synthesized complexes, their UV-Vis absorption spectrum was recorded in MeCN and compared with the one of complex **1** (Fig. 3). As shown in Fig. 3, every complex displays an absorption band in the UV (290 nm) corresponding to bipyridine-centred transitions, with a 10 nm bathochromic shift in the case of the bipyrazine-coordinated complex **8**. The complexes display a second band in the near-visible region corresponding to distyryl ligands-centred transitions. Both the position and the nature of the ligand influenced this absorption band. A bathochromic shift was observed with electron-donating group-substituted ligands (*i.e.*, OMe, NH_2, and OH) compared to electron-withdrawing groups (*i.e.*,

NO_2, F). The effects were however modest on the absorption band in the visible region corresponding to metal to ligand centred transitions. A 50 nm hypsochromic shift was observed in the case of complex **8**. Interestingly, a slight bathochromic shift was observed in complex **7**, in which the electron-donating OMe group was replaced with an electron-withdrawing NO_2 group. Finally, a characteristic broad absorption band (550-750 nm) was observed for the Os derivative, corresponding to spin forbidden metal to ligand centred transitions as described in previous studies.[22,25]

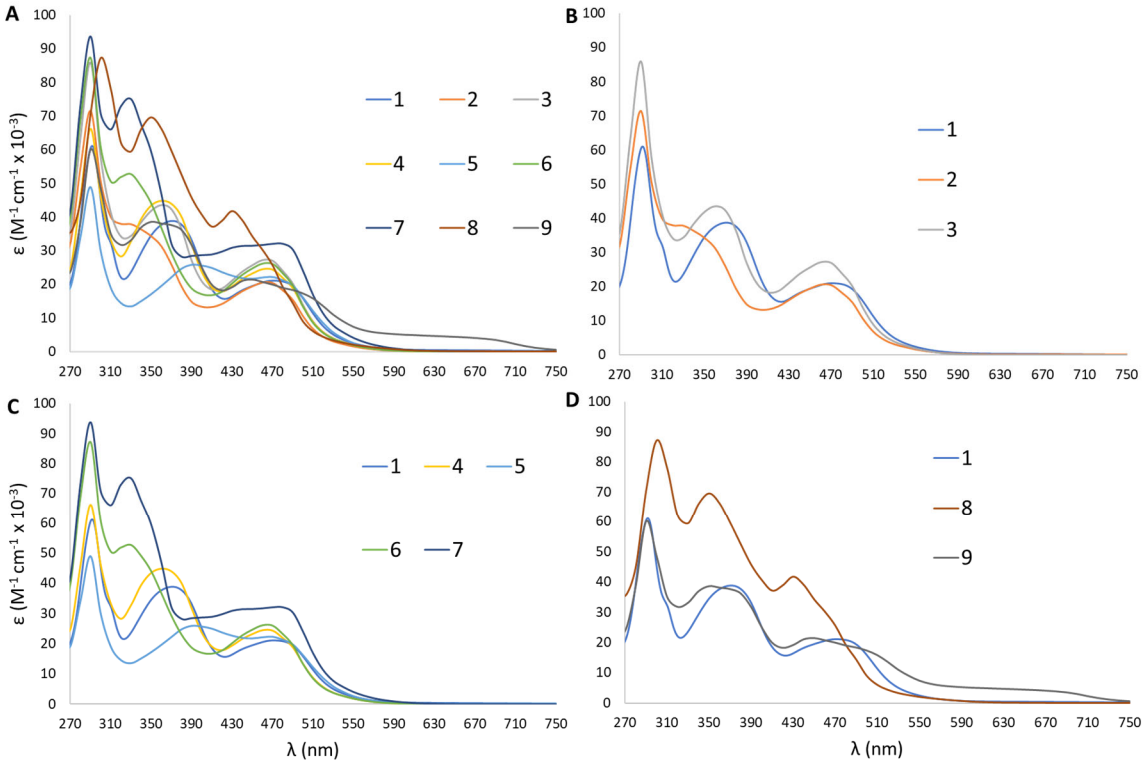

Figure 3. Complexes **1–9** UV-Vis absorption spectra measured in MeCN. **A.** Superimposed spectra; **B.** Comparison of the effect of the OMe substituent position; **C.** Comparison of the effect of electron-donating or withdrawing groups at the *para* position; **D.** Comparison of the effect of the replacement of the metal centre or of the bipyridine ligand.

Hydrophobicity

The lipophilicity of one drug can often be correlated to its plasma membrane penetration and to its eventual absorption, biodistribution and disposition.[26,27] For this reason, the partition coefficients between water and octanol, also known as Log *P*, of the complexes were determined by the shake-flask method. PBS (pH = 7.4) was used instead of water to normalize the effect of pH on the complexes' lipophilicity. As shown in Fig. 4, all compounds were found to be lipophilic, with a preferential partition in the octanol layer. The OMe group position had a slight effect on the lipophilicity of the complexes in the order *m*-OMe > *o*-OMe > *p*-OMe. As expected, hydrophobic substituents or groups able to form hydrogen bonds had a significant effect on the Log *P* in the order F > OMe > OH > NH_2. On the contrary, replacing the two 2,2'-bipyridine ligands by 2,2'-bipyrazine ligands failed at improving the complex's hydrophilicity. Finally, the heavy Os nucleus slightly increased the complex's Log *P*. The Log *P* of complex **7** could not be precisely measured using this method due to its poor solubility in both phases.

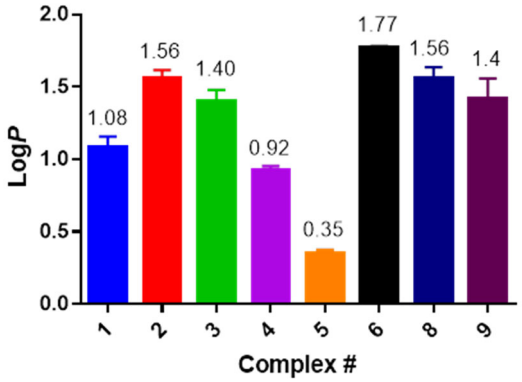

Figure 4. Octanol/PBS partition coefficients of complexes **1**-**6**, **8** and **9**.

Of note, in our previous study, the Log *P* of complex **1** as a chloride salt was measured as 0.5, which shows than the exchange of the counter ion could further increase the complexes' hydrophilicity.[12]

Singlet oxygen production

The ability of the synthesised complexes to produce singlet oxygen ($^1O_2$) upon irradiation at 450 nm in MeCN and D_2O was evaluated by direct observation of $^1O_2$ phosphorescence at about 1270 nm using phenalenone or $[Ru(bipy)_3]Cl_2$ as references, respectively. As shown in Tab. 1, structural variations on complex **1** only had minor effects on the compound's ability to sensitise O_2, although a significant decrease in the quantum yield could be observed for complex **8**. Nevertheless, all complexes demonstrated the potential to generate $^1O_2$, which can cause oxidative damage in tissue. Notably, with our experimental setup, only singlet oxygen quantum yields higher than 0.2 can be observed. The absence of $^1O_2$ phosphorescence signal in D_2O is the indication that the $^1O_2$ production of these PSs is below this threshold. Previous investigations have shown that this observation does not hamper the generation of a phototoxic effect in cancerous cells.

Table 1. Singlet oxygen quantum yields of studied complexes measured in MeCN and D_2O. N.D.: Not Detected.

Complex	ϕ^1O_2(MeCN)	ϕ^1O_2(D_2O)
1	0.37	N.D.
2	0.38	N.D.
3	0.47	N.D.
4	0.31	N.D.
5	0.50	N.D.
6	0.53	N.D.
7	0.35	N.D.
8	0.25	N.D.
9	0.45	N.D.

Cellular uptake

Since the biological efficiency is highly dependent on the PS ability to be taken up by the cell, the cellular uptake of each complex was determined in HeLa (human cervical adenocarcinoma) cells by inductively coupled plasma mass spectrometry following 4 hours of incubation with 5 µM of the complexes. The results gathered in Fig. 5 show that all tested complexes except **5** and **7** share similar uptake levels.

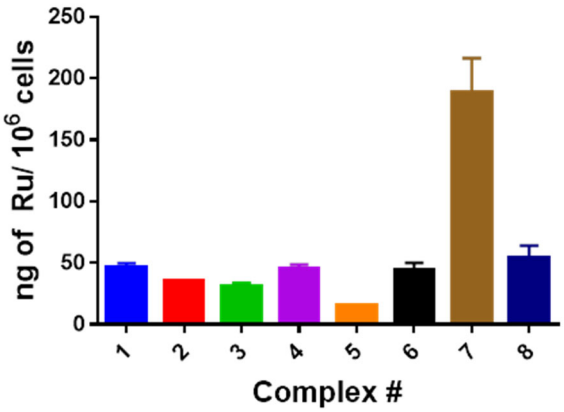

Figure 5. Ruthenium content in HeLa cells following 4 hours of incubation with 5 µM of complexes **1**-**8**.

Complex **5** displayed a reduced uptake compared to the other derivatives, which could be due to its reduced lipophilicity, as low lipophilicity is generally correlated to poor plasma membrane penetration.[26] The cellular uptake of complex **7** was found to be about 4 times higher compared to complex **1**, which could again be linked to a higher lipophilicity, although this could not be precisely determined during the partition experiment.

Phototoxicity

In order to evaluate the potential of the complexes as PDT agents, their toxicity in the dark or upon light irradiation at 480 nm was evaluated on HeLa and RPE-1 (normal human epithelial cells immortalized with hTERT) cells, following incubation for 4 hours with increasing concentrations of the complexes. The concentration needed to reduce the cell viability to 50% (IC_{50}) is presented in Tab.2. Of note, all compounds were found to be non-toxic in the dark (>100 µM) except **3** which demonstrated a slight cytotoxicity. In the case of complex **7**, insoluble aggregates were observed at the highest concentration tested (100 µM). The complex appeared however fully soluble in the culture medium at 30 µM and below. For comparative purposes, a bar graph representation can be found in the supplementary information (Fig. S22).

	IC_{50} (µM)					
	HeLa			RPE-1		
Compound	dark	480 nm, 10 min 3.2 J/cm²	PI	dark	480 nm, 10 min 3.2 J/cm²	PI
1	>100	0.56 ± 0.07	179	>100	1.6 ± 0.2	>63
2	>100	0.6 ± 0.3	>167	>100	1.6 ± 0.2	>63

3	62 ± 10	0.5 ± 0.1	124	>100	1.52 ± 0.09	>66
4	>100	1.0 ± 0.3	>100	>100	11 ± 2	>9
5	>100	1.4 ± 0.1	>71	>100	8 ± 1	>13
6	>100	0.8 ± 0.1	>125	>100	1.47 ± 0,06	>68
7	>100	4 ± 1	>25	>100	15 ± 1	>7
8	>100	59 ± 8	>2	>100	>100	ND
9	>100	27 ± 6	4	>100	30 ± 7	>3

Table 2. Cytotoxicity (dark) and phototoxicity of complexes **1**-**9** on HeLa and RPE-1 cells after 4 h of incubation and upon irradiation at 480 nm for 10 min (3.2 J/cm²).

Complexes **1**-**6** showed similar and high phototoxicities, with IC_{50} in the range 0.5-1.4 µM and good phototoxicity indexes (PI = IC_{50}(dark)/IC_{50}(light)) higher than 167 for complex **1** and **2**. Interestingly, complexes **1**-**3** had a similar phototoxicity on cancerous (HeLa) and on normal (RPE-1) cells, whereas complexes **4** and **5** seemed significantly less toxic on normal cells. On the other hand, complexes **7**-**9** were found to be significantly less phototoxic compared to complex **1**. In particular, complex **8** was found to be only slightly phototoxic, with IC_{50}s of 59 and >100 on HeLa and RPE-1 cells respectively. This result could be due to lower singlet oxygen production, in line with the lower quantum yield measured for this complex (see Tab. 1).

CONCLUSIONS

This structure-activity relationship study demonstrated that subtle structural modifications on a given ligand can lead to significant changes in the corresponding complex's physical and biological properties. Some of these effects were to be expected. In particular, the introduction of hydrophilic groups on the distyryl ligand's phenyl ring had a positive effect on the hydrophilicity of complexes **4** and **5**. However, most of the structural modifications had somewhat unexpected or counterintuitive effects on the final complexes. The introduction of a nitro substituent in **7** led to a significant decrease in its aqueous solubility. On the other hand, the introduction of this electron-withdrawing substituent did not lead to a significant and detrimental hypsochromic shift in the metal to ligand centred transitions related absorption band compared to electron-donating substituents, as was postulated before. This is also the case in **6**, also it is generally admitted that the inductive effects in para-substituted fluorobenzene derivatives are compensated by mesomeric effects.[28] Additionally, the superior cellular uptake of **7** did not confer a superior phototoxicity to this complex. Moreover, the introduction of bipyrazine ligands, able to interact with water through hydrogen bonding, did not improve complex **8** hydrophilicity, although it appeared to affect negatively its $^1O_2$ quantum yield, and therefore its phototoxicity. Finally, the replacement of the Ru centre by an Os centre in **9** had a detrimental effect on the complex's phototoxicity, although it unlocked the possibility to excite it at up to 750 nm. It is important to note that, at this stage, other features (*e.g.* (photo)stability, subcellular localization…) could significantly affect the eventual phototoxicity of the complexes. Overall, this study highlights the crucial importance of empirical characterisations over mere simulations and provides some guidance on how to design new Ru-based PSs. Importantly, **4** and **5** displayed a similar phototoxicity in comparison to **1** on cancer cells but appeared less phototoxic on normal cells. Additionally, they displayed

an improved hydrophilicity, which could lead to better pharmacological properties. These two complexes appear therefore as good candidates for further developments.

EXPERIMENTAL SECTION

Materials

All chemicals were obtained from commercial sources and were used without further purification.

Instrumentation and methods

^{1}H- and ^{13}C-NMR spectra were recorded on a 400 MHz NMR spectrometer (Bruker). Chemical shifts (δ) are reported in parts per million (ppm) referenced to tetramethylsilane (δ 0.00) ppm using the residual proton solvent peaks as internal standards. Coupling constants (*J*) are reported in Hertz (Hz) and the multiplicity is abbreviated, as follows: s (singlet), d (doublet), and m (multiplet). Electrospray Ionization-Mass Spectrometry (ESI-HRMS) experiments were carried out using a LTQ-Orbitrap XL from Thermo Scientific (Thermo Fisher Scientific) and operated in positive ionization mode, with a spray voltage at 3.6 kV. No sheath and auxiliary gas was used. Applied voltages were 40 and 100 V for the ion transfer capillary and the tube lens, respectively. The ion transfer capillary was held at 275 °C. Detection was achieved in the Orbitrap with a resolution set to 100,000 (at *m/z* 400) and an *m/z* range between 150 and 2000 in profile mode. Spectrum was analyzed using the acquisition software XCalibur 2.1 (Thermo Fisher Scientific). The automatic gain control (AGC) allowed for the accumulation of up to $2{\cdot}10^{5}$ ions for Fourier Transform Mass Spectrometry (FTMS) scans, maximum injection time was set to 300 ms and 1 µs scan was acquired. 10 µL was injected using a Thermo Finnigan Surveyor HPLC system (Thermo Fisher Scientific) with a continuous infusion of methanol at 100 $\mu L{\cdot}min^{-1}$. Elemental microanalyses were performed on a Thermo Flash 2000 elemental analyzer.

Synthesis

The ligand (*E*,*E*')-4,4´-Bis[*p*-methoxystyryl]-2,2´-bipyridine and complex **1** were synthesized in a previous study and used without further purification.[12] Dichlorobis(bipyridine)ruthenium(II) ($Ru(bpy)_2Cl_2$), dichlorobis(bipyrazine)ruthenium(II) ($Ru(bpz)_2Cl_2$), dichlorobis(bipyridine)osmium (II) ($Os(bpy)_2Cl_2$), (*E*,*E*')-4,4´-Bis[*p*-hydroxystyryl]-2,2´-bipyridine and (*E*,*E*')-4,4´-Bis[*p*-nitrostyryl]-2,2´-bipyridine were synthesized as reported in the literature.[23,29–31]

<u>Synthesis of the ligands:</u>

(*E*,*E*')-4,4´-Bis[*m*-methoxystyryl]-2,2´-bipyridine

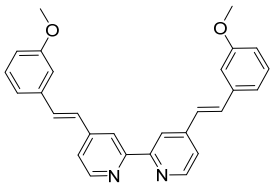

The synthesis of (*E*,*E*')-4,4´-Bis[*m*-methoxystyryl]-2,2´-bipyridine has already been described but in this study another synthetic route was employed.[32] 4,4´-Dimethyl-2,2´-bipyridine (4.95 g, 26.9 mmol, 1.0 equiv.) was dissolved in dry DMF (100 mL) under nitrogen atmosphere and 3-methoxybenzaldehyde (7.2 mL, 59.1 mmol, 2.2 equiv.) was added to the solution. Afterwards potassium *tert*-butoxide (12.05 g, 107.0 mmol, 4.0 equiv.) was added slowly and the mixture was stirred for 24 h. The mixture was then poured into H_2O (200 mL) and the suspension cooled down to 5 °C. The crude product which precipitated, was filtered, and washed with methanol. The product was purified by recrystallization from boiling acetic acid. The obtained solid was dissolved in Dichloromethane and the mixture was washed with a 5% LiCl aqueous solution, brine, and H_2O. The solvent was removed to yield (*E*,*E*')-4,4´-Bis[*m*-methoxystyryl]-2,2´-bipyridine as a beige solid (8.69 g, 20.7 mmol, 77%). Spectroscopic data were in accordance with the literature.

(*E*,*E*')-4,4´-Bis[*o*-methoxystyryl]-2,2´-bipyridine

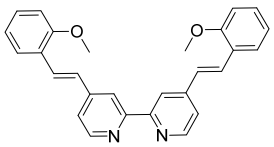

The synthesis of (*E*,*E*')-4,4´-Bis[*o*-methoxystyryl]-2,2´-bipyridine has already been described but in this study another synthetic route was employed.[33] 4,4´-Dimethyl-2,2´-bipyridine (1.00 g, 5.43 mmol, 1.0 equiv.) was dissolved in dry DMF (50 mL) under nitrogen atmosphere and 4-methoxybenzaldehyde (1.63 mL, 13.57 mmol, 2.5 equiv.) was added to the solution. Afterwards potassium *tert*-butoxide (2.44 g, 21.74 mmol, 4.0 equiv.) was added slowly and the mixture was stirred for 24 h. The mixture was then poured into H_2O (500 mL) and the suspension cooled down to 5 °C. The crude product which precipitated, was filtered, and washed with methanol. The product was purified by recrystallization from chloroform to yield (*E*,*E*')-4,4´-Bis[*p*-methoxystyryl]-2,2´-bipyridine as a beige solid (1.85 g, 4.40 mmol, 81%). Spectroscopic data were in accordance with the literature.

(*E*,*E*')-4,4´-Bis[*p*-aminostyryl]-2,2´-bipyridine

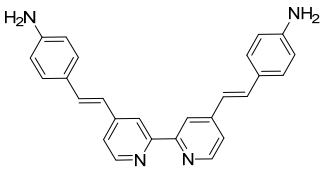

The synthesis of (*E*,*E*')-4,4´-Bis[*p*-aminostyryl]-2,2´-bipyridine has already been described.[34] However in this study, (*E*,*E*')-4,4´-Bis[*p*-aminostyryl]-2,2´-bipyridine was synthesized by sodium dithionite-mediated reduction of (*E*,*E*')-4,4´-Bis[*p*-nitrostyryl]-2,2´-bipyridine. Under nitrogen, (*E*,*E*')-4,4´-Bis[*p*-aminostyryl]-2,2´-bipyridine (450 mg, 1.0 mmol, 1 equiv.) and sodium dithionite (1.22 g, 7.0 mmol, 7.0 equiv.) were dissolved in DMSO (10 mL). Distilled water (1 mL) was added, and the mixture was heated at 90 °C for 15 h. The mixture was then cooled down and poured in water (100 mL). $NaHCO_3$ saturated in water was added to adjust the suspension pH to 7 and the mixture was agitated for 10 min. The solid was then filtered and washed with cold water, followed by cold ethanol and diethyl ether, and then dried under vacuum to yield a yellow powder (183 mg, 0.46 mmol, 46%). Spectroscopic data were in accordance with the literature.

(*E*,*E*')-4,4´-Bis[*p*-fluorostyryl]-2,2´-bipyridine

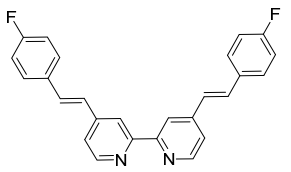

4,4´-Dimethyl-2,2´-bipyridine (1.00 g, 5.43 mmol, 1.0 equiv.) was dissolved in dry DMF (50 mL) under nitrogen atmosphere and 4-fluorobenzaldehyde (1.46 mL, 13.57 mmol, 2.5 equiv.) was added to the solution. Afterwards potassium *tert*-butoxide (2.44 g, 21.74 mmol, 4.0 equiv.) was added slowly. The colour of the solution turned to green, and the mixture was stirred for 24 h. After that the mixture which turned bright was poured into H_2O (500 mL) and the suspension cooled down to 5 °C. The crude product which precipitated, was filtered, and washed with methanol. The product was purified by recrystallization from boiling acetic acid. The obtained solid was dissolved in Dichloromethane and the mixture was washed with a 5% LiCl aqueous solution, brine, and H_2O. The solvent was removed to yield (*E*,*E*')-4,4´-Bis[*p*-fluorostyryl]-2,2´-bipyridine as a beige solid (1.38 g, 3.48 mmol, 64 %). ^{1}H-NMR (400 MHz, CD_2Cl_2): δ 8.75 (dd, *J* = 5.0, 0.7 Hz, 2H), 8.68 (dd, *J* = 1.7, 0.7 Hz, 2H), 7.69 (dd, *J* = 8.7, 5.3 Hz, 4H), 7.55 (d, *J* = 16.5 Hz, 2H), 7.52 (dd, *J* = 5.0, 1.7 Hz, 2H), 7.22 (dd, *J* = 8.7, 5.3 Hz, 4H), 7.20 (d, *J* = 16.5 Hz, 2H); ESI-HRMS (positive detection mode): calcd for $C_{26}H_{19}N_2F_2$, 397.1516; found, 397.1513.

<u>Synthesis of the complexes:</u>

General procedure

Under nitrogen, $Ru(bpy)_2Cl_2$ (1.0 equiv., for complexes **2**-**7**), $Ru(bpz)_2Cl_2$ (1.0 equiv., for complex **8**) or $Os(bpy)_2Cl_2$ (1.0 equiv., for complex **9**) and the corresponding ligand (1.2 equiv.) were heated in EtOH (80 °C, 6 h) or ethylene glycol (130 °C, 24 h). Then the solution was cooled down to room temperature and a saturated aqueous solution of NH_4PF_6 was added. The crude product, which precipitated as a PF_6 salt, was collected by filtration and washed with water and diethyl ether. When indicated, the crude product was purified by silica gel chromatography using acetonitrile/potassium nitrate 0.3 M in water (9:1 v/v) as eluent. The fractions containing the product were collected and the solvent evaporated. The residue was dissolved in acetonitrile and filtered. The filtrate was concentrated to dryness under vacuum. The residue was dissolved in ethanol and a saturated aqueous solution of NH_4PF_6 was added. The precipitate was filtered, washed with water and diethyl ether, and dried under vacuum.

$[Ru(bpy)_2((E,E')$-4,4´-Bis[*m*-methoxystyryl]-2,2´-bipyridine)$][PF_6]_2$ (**2**)

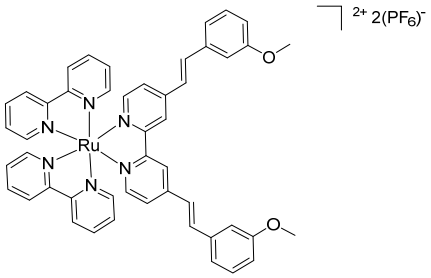

Synthesized from $Ru(bpy)_2Cl_2$ and (*E*,*E*')-4,4´-Bis[*m*-methoxystyryl]-2,2´-bipyridine on a 0.41 mmol scale in EtOH (50 mL). **2** was obtained without purification as a dark red solid (390 mg, 0.35 mmol, 85%). ^{1}H-NMR (400 MHz, CD_3CN): δ 8.72 (d, *J* = 1.9 Hz, 2H), 8.52 (d, *J* = 8.2 Hz, 4H), 8.07 (td, *J* = 7.9, 1.5, 4H), 7.85 (d, *J* = 5.6 Hz, 2H), 7.78-7.61 (m, 6H), 7.54-7.09 (m, 14H), 6.95 (dd, *J* = 7.3, 1.9, 2H), 3.84 (s, 6H). ^{13}C-NMR ($CDCl_3$, 101 MHz): δ = 161.2, 158.2, 158.0, 152.7, 152.4, 147.6, 138.8, 138.3, 137.2, 131.1, 128.6, 125.4, 125.3, 125.2, 121.7, 121.3, 116.4, 113.2, 56.0. ESI-HRMS (positive detection mode): calcd for $C_{48}H_{40}N_6O_2Ru$ m/z $[M]^{2+}$ 417.1128; found: 417.1126. Elemental analysis calcd for $C_{48}H_{40}F_{12}N_6O_2P_2Ru$ (%): C 51.30, H 3.59, N 7.48; found: C 51.06, H 3.61, N 7.38.

$[Ru(bpy)_2((E,E')$-4,4´-Bis[*o*-methoxystyryl]-2,2´-bipyridine)$][PF_6]_2$ (**3**)

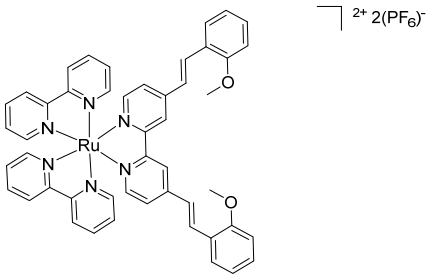

Synthesized from $Ru(bpy)_2Cl_2$ and (*E*,*E*')-4,4´-Bis[*o*-methoxystyryl]-2,2´-bipyridine on a 0.31 mmol scale in EtOH (50 mL). **3** was obtained without purification as a dark red solid (225 mg, 0.20 mmol, 65%). ^{1}H-NMR (400 MHz,CD_3CN): δ 8.71 (d, *J* = 1.9 Hz, 2H), 8.59-8.33 (m, 4H), 8.07 (m, 4H), 7.95 (d, *J* = 16.5 Hz, 2H), 7.84 (d, *J* = 4.3 Hz, 2H), 7.74 (ddd, *J* = 5.6, 1.5, 0.8 Hz, 2H), 7.68 (dd, *J* = 7.7, 1.7 Hz, 2H), 7.61 (d, *J* = 6.0 Hz, 2H), 7.42 (m, 10H), 7.06 (m, 4H), 3.94 (s, 6H). ^{13}C-NMR ($CDCl_3$, 101 MHz): δ = 158.9, 158.2, 158.0, 152.6, 152.2, 148.3, 138.7, 132.7, 132.0, 129.0, 128.5, 125.8, 125.4, 125.2, 125.0, 121.9, 121.8, 112.6, 56.3. ESI-HRMS (positive detection mode): calcd for $C_{48}H_{40}N_6O_2Ru$ m/z $[M]^{2+}$ 417.1128; found: 417.1126. Elemental analysis calcd for $C_{48}H_{40}F_{12}N_6O_2P_2Ru+H_2O$ (%): C 50.49, H 3.71, N 7.36; found: C 50.27, H 3.41, N 7.66.

$[Ru(bpy)_2$((*E*,*E*')-4,4´-Bis[*p*-hydroxystyryl]-2,2´-bipyridine)$][PF_6]_2$ (**4**)

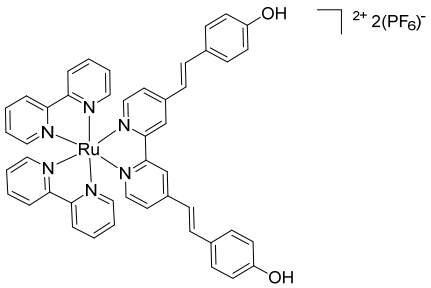

Synthesized from $Ru(bpy)_2Cl_2$ and (*E*,*E*')-4,4´-Bis[*p*-hydroxystyryl]-2,2´-bipyridine on a 0.31 mmol scale in ethylene glycol (5 mL). **4** was obtained without purification as a dark red solid (297 mg, 0.27 mmol, 87%). ^{1}H-NMR (CD_3CN, 400 MHz): δ = 8.66 (d, *J* = 1.9 Hz, 2H), 8.50 (d, *J* = 8.1 Hz, 4H), 8.05 (td, *J* = 8.0, 1.5 Hz, 4H), 7.84 (d, *J* = 5.1 Hz, 2H), 7.74 (d, *J* = 5.0 Hz, 2H), 7.68 (d, *J* = 16.4 Hz, 2H), 7.61 - 7.51 (m, 6H), 7.46 - 7.35 (m, 8H), 7.12 (d, *J* = 16.5 Hz, 2H), 6.90 (d, *J* = 8.6 Hz, 4H). ^{13}C-NMR (CD_3CN, 101 MHz): δ = 159.5, 158.01, 157.95, 152.6, 152.1, 148.2, 138.6, 137.3, 130.2, 128.7, 128.5, 125.1, 124.9, 122.1, 121.2, 116.9. ESI-HRMS (positive detection mode): calcd for $C_{46}H_{36}N_6O_2Ru$ m/z $[M]^{2+}$ 403.0972; found: 403.0970. Elemental analysis calcd for $C_{46}H_{36}F_{12}N_6O_2P_2Ru+H_2O$ (%): C 49.60, H 3.44, N 7.55; found: C 49.46, H 3.35, N 7.31.

$[Ru(bpy)_2$((*E*,*E*')-4,4´-Bis[*p*-aminostyryl]-2,2´-bipyridine)$][PF_6]_2$ (**5**)

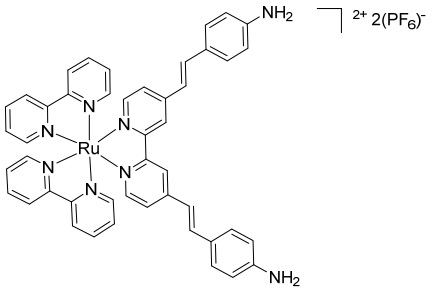

Compound **5** was synthesized following a procedure described in the literature.[24] Spectroscopic data were in accordance with the literature. Elemental analysis calcd for $C_{46}H_{38}F_{12}N_8P_2Ru+3H_2O$ (%): C 48.13, H 3.86, N 9.76; found: C 48.09, H 3.37, N 10.05.

[Ru(bpy)$_2$((*E*,*E*')-4,4´-Bis[*p*-fluorostyryl]-2,2´-bipyridine)][PF_6]$_2$ (**6**)

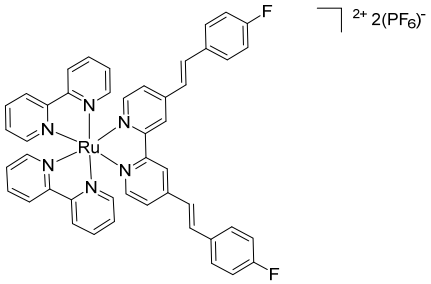

Synthesized from Ru(bpy)$_2$Cl$_2$ and (*E*,*E*')-4,4´-Bis[*p*-fluorostyryl]-2,2´-bipyridine on a 0.50 mmol scale in EtOH (50 mL). **6** was obtained after silica gel purification as a dark red solid (273 mg, 0.29 mmol, 57%). ^{1}H-NMR (CD_3CN, 400 MHz): δ = 8.72 (d, *J* = 1.9 Hz, 2H), 8.53 (d, *J* = 8.2 Hz, 4H), 8.07 (t, *J* = 7.9 Hz, 4H), 7.85 (d, *J* = 5.6 Hz, 2H), 7.80 - 7.68 (m, 8H), 7.65 (d, *J* = 6.0 Hz, 2H), 7.52-7.36 (m, 6H), 7.26 (d, *J* = 16.5 Hz, 2H), 7.19 (d, *J* = 8.8 Hz, 4H). ^{13}C-NMR (CD_3CN, 101 MHz): δ = 164.3 (d, $^1J_{C-F}$ = 248 Hz), 158.2, 158.0, 158.0, 152.7, 152.4, 147.6, 138.8, 136.0, 133.4 (d, $^4J_{C-F}$ = 3 Hz), 130.5 (d, $^3J_{C-F}$ = 8 Hz), 128.6, 125.2, 125.0, 121.8, 116.9 (d, $^2J_{C-F}$ = 22 Hz). ^{19}F NMR (376 MHz, CD_3CN) δ = -72.77 (d, *J* = 706.7 Hz), -112.83. ESI-HRMS (positive detection mode): calcd for $C_{46}H_{34}N_6F_2Ru$ m/z $[M]^{2+}$ 405.0928; found: 405.0927. Elemental analysis calcd for $C_{46}H_{34}F_{14}N_6O_2P_2Ru+H_2O$ (%): C 49.43, H 3.25, N 7.52; found: C 49.76, H 3.02, N 7.47.

[Ru(bpy)$_2$((*E*,*E*')-4,4´-Bis[*p*-nitrostyryl]-2,2´-bipyridine)][PF_6]$_2$ (**7**)

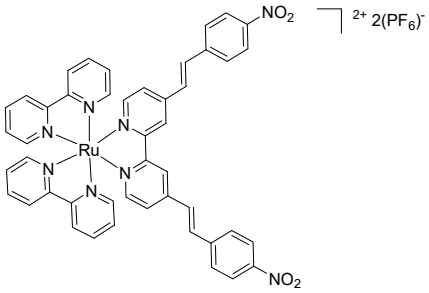

Synthesized from $Ru(bpy)_2Cl_2$ and (*E*,*E*')-4,4´-Bis[*p*-nitrostyryl]-2,2´-bipyridine on a 0.31 mmol scale in ethylene glycol (5 mL). **7** was obtained without purification as a dark red solid (276 mg, 0.24 mmol, 77%). ^{1}H-NMR (CD_3CN, 400 MHz): δ = 8.78 (d, *J* = 1.9 Hz, 2H), 8.53 (dt, *J* = 8.3, 1.1 Hz, 4H), 8.23 (d, *J* = 8.9 Hz, 4H), 8.08 (tdd, *J* = 8.0, 2.5, 1.5 Hz, 4H), 7.87 - 7.83 (m, 6H), 7.80 - 7.71 (m, 6H), 7.52 (dd, *J* = 6.0, 1.8 Hz, 2H), 7.49 - 7.39 (m, 6H). ^{13}C-NMR (CD_3CN, 101 MHz): δ = 158.3, 157.88, 152.7, 152.6, 148.8, 146.6, 143.1, 138.8, 134.6, 129.3, 129.1, 128.6, 125.6, 125.2, 125.1, 122.1. ESI-HRMS (positive detection mode): calcd for $C_{46}H_{34}O_4N_8Ru$ m/z $[M]^{2+}$ 432.0873; found: 432.0871. Elemental analysis calcd for $C_{46}H_{34}F_{12}O_4N_8P_2Ru$ (%): C 47.88, H 2.97, N 9.71; found: C 47.73, H 2.78, N 9.41.

$[Ru(bpz)_2$((*E*,*E*')-4,4´-Bis[*p*-methoxystyryl]-2,2´-bipyridine)$][PF_6]_2$ (**8**)

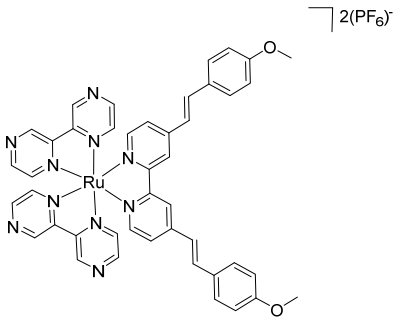

Synthesized from $Ru(bpz)_2Cl_2$ and (*E*,*E*')-4,4´-Bis[*p*-methoxystyryl]-2,2´-bipyridine on a 0.21 mmol scale in ethylene glycol (5 mL). **8** was obtained after silica gel purification as a dark red solid (43 mg, 0.04 mmol, 19%). ^{1}H-NMR (CD_3CN, 400 MHz): δ = 9.76 (t, *J* = 1.5 Hz, 4H), 8.71 (d, *J* = 1.9 Hz, 2H), 8.61 (dd, *J* = 9.8, 3.2 Hz, 4H), 7.90 (dd, *J* = 3.3, 1.2 Hz, 2H), 7.87 (dd, *J* = 3.2, 1.2 Hz, 2H), 7.76 (d, *J* = 16.4 Hz, 2H), 7.66 (d, *J* = 8.9 Hz, 4H), 7.54 (d, *J* = 6.0 Hz, 2H), 7.48 (dd, *J* = 6.1, 1.8 Hz, 2H), 7.19 (d, *J* = 16.3 Hz, 2H), 7.03 (d, *J* = 8.8 Hz, 4H), 3.85 (s, 6H). ^{13}C-NMR (CD_3CN, 101 MHz): δ = 162.2, 157.2, 152.6, 151.7, 149.7, 149.34, 149.30, 147.9, 147.3, 146.1, 138.0, 130.2, 129.2, 125.3, 122.2, 121.6, 115.5, 56.1. ESI-HRMS (positive detection mode): calcd for $C_{44}H_{36}N_{10}O_2Ru$ m/z $[M]^{2+}$ 419.1033; found: 419.1030. Elemental analysis calcd for $C_{44}H_{36}F_{12}N_{10}O_2P_2Ru+4H_2O$ (%): C 44.04, H 3.70, N 11.67; found: C 44.11, H 2.95, N 11.60.

$[Os(bpy)_2$((*E*,*E*')-4,4´-Bis[*p*-methoxystyryl]-2,2´-bipyridine)$][PF_6]_2$ (**9**)

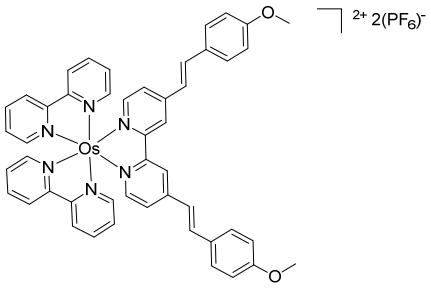

Synthesized from $Os(bpy)_2Cl_2$ and (*E*,*E*')-4,4´-Bis[*p*-methoxystyryl]-2,2´-bipyridine on a 0.17 mmol scale in degassed ethylene glycol (5 mL). **9** was obtained without purification as a dark brown solid (189 mg, 0.16 mmol, 94%). ^{1}H-NMR (CD_3CN, 400 MHz): δ = 8.64 (d, *J* = 2.0 Hz, 2H), 8.49 (d, *J* = 8.0 Hz, 4H), 7.86 (ddt, *J* = 9.7, 8.2, 1.7 Hz, 4H), 7.74 (d, *J* = 5.4 Hz, 2H), 7.71 - 7.59 (m, 8H), 7.50 (d, *J* = 6.1 Hz, 2H), 7.38 - 7.26 (m, 6H), 7.16 (d, *J* = 16.3 Hz, 2H), 7.02 (d, *J* = 8.8 Hz, 4H), 3.84 (s, 6H). ^{13}C-NMR (CD_3CN, 101 MHz): δ = 162.0, 159.97, 159.92, 159.87, 151.8, 151.7, 151.3, 147.5, 138.0, 137.2, 130.1, 129.3, 129.0, 125.4, 125.2, 122.2, 121.4, 115.4. ESI-HRMS (positive detection mode): calcd for $C_{48}H_{40}N_6O_2Os$ m/z $[M]^{2+}$ 462.1414; found: 462.1406. Elemental analysis calcd for $C_{48}H_{40}F_{12}N_6O_2OsP_2+H_2O$ (%): C 46.83, H 3.44, N 6.83; found: C 46.92, H 3.29, N 6.34.

positive detection positive detection positive detection positive detection positive detection positive detection positive detection positive detection

Spectroscopic measurements

The absorption of the samples was measured with a Cary 4000 UV-Vis spectrophotometer (Agilent).

Singlet oxygen production measurement

The samples were prepared in an air saturated CH_3CN or D_2O solution with an absorbance of 0.2 at 450 nm. This solution was irradiated in fluorescence quartz cuvettes (width 1 cm) using a mounted M450LP1 LED (Thorlabs) whose irradiation, centered at 450 nm, has been focused with aspheric condenser lenses. The intensity of the irradiation has been varied using a T-Cube LED Driver (Thorlabs) and measured with an optical power and energy meter. The emission signal was focused and collected at right angle to the excitation pathway and directed to a Princeton Instruments Acton SP-2300i monochromator. A longpass glass filter was placed in front of the monochromator entrance slit to cut off light at wavelengths shorter than 850 nm. As a detector an EO-817L IR-sensitive liquid nitrogen cooled germanium diode detector (North Coast Scientific Corp.) has been used. The singlet oxygen luminesce at 1270 nm was measured by recording spectra from 1100 to 1400 nm. For the data analysis, the singlet oxygen luminescence peaks at different irradiation intensities were integrated. The resulting areas were plotted against the percentage of the irradiation intensity and the slope of the linear regression calculated. The absorbance of the sample was corrected with an absorbance correction factor. As reference for the measurement Phenalenone (ϕ^1O_2(MeCN)= 95%)[35] and

$[Ru(bipy)_3Cl_2]$ ($\phi^1O_2(D_2O)$= 22%)[36] were used in acetonitrile and D_2O respectively and the singlet oxygen quantum yields were calculated using the following formula:

$\phi_{sample} = \phi_{reference} * (S_{sample} / S_{reference}) * (I_{reference} / I_{sample})$

$I = I_0 * (1 - 10^{-A})$

ϕ = singlet oxygen quantum yield, S = slope of the linear regression of the plot of the areas of the singlet oxygen luminescence peaks against the irradiation intensity, I = absorbance correction factor, I_0 = light intensity of the irradiation source, A = absorbance of the sample at the irradiation wavelength.

Of note, for ruthenium complexes, the singlet oxygen luminescence peaks were integrated between 1220 and 1350 nm. For the osmium complex **9**, the luminescence peak was integrated between 1250 and 1300 nm to reduce the impact of the complex intrinsic luminescence at these wavelengths.

Distribution coefficient measurement

Octanol and PBS were saturated with each other by continuous mixing at room temperature for 24 h. The test compounds were dissolved at a concentration of ca. 200 µM in 1 mL of the octanol phase. An equal volume of the PBS phase was added, and the mixture was agitated at room temperature for 24 h. The two layers were separated, and the absorbance of each layer was determined at 450 nm. The log *P* values were determined as follows:

$$Log\ P = Log\ (\frac{Abs_{450}(Octanol)}{Abs_{450}(PBS)})$$

Cell culture

HeLa cells were cultured in DMEM media (Gibco, Life Technologies, USA) supplemented with 10 % of fetal calf serum (Gibco). RPE-1 cells were cultured in DMEM/F-12 (Gibco) supplemented with 10 % of fetal calf serum. All cell lines were complemented with 100 U/mL penicillin-streptomycin mixture (Gibco) and maintained in an humidified atmosphere at 37 °C and 5 % of CO_2.

Cellular uptake

HeLa cells were seeded at a 1.10^6 cells/well density in 6-well-plates (1 mL/well) and were incubated at 37 °C, 5% CO_2. The next day, the medium was replaced with 5 µM of test compounds dilutions in medium and cells were incubated for an additional 4 h at 37 °C, 5% CO_2. Cells were then washed three times with cold PBS, trypsinized, harvested, and a 10 µL aliquot of each cell suspension was sampled for accurate counting. The cell suspensions were centrifuged, and the supernatant was discarded. The pellets were digested in 100 µL of 70% HNO_3 at 65 °C for 24 h and then diluted in 5 mL of MilliQ water (final HNO_3 concentration: 1.4 %). The Ru content in each sample was determined by ICP-MS. Data are presented as a mean of three independent replicates.

Phototoxicity

Cells were seeded at a 4,000 cells/well density in 96-well plates (100 µL/well) and were incubated at 37 °C, 5% CO_2 for 24 h. The medium was replaced by test compound dilutions in fresh medium (100 µL/well) and cells were incubated at 37 °C, 5% CO_2 for 4 h. The medium was replaced by 100 µL of fresh medium. Plates were then irradiated at 480 nm for 10 min at 37 °C (3.2 J/cm²) using a LUMOS-BIO photoreactor (Atlas Photonics)**.** As a control, a plate was kept in the dark for 10 min at 37°C, 0% CO_2. Cells were then incubated for an additional 44 h at 37 °C, 5% CO_2. The medium was replaced with 100 µL of fresh medium containing resazurin (0.2 mg/mL). After 4h of incubation at 37 °C, 5% CO_2, plates were read using a SpectraMaxM2 Microplate Reader (λ_{exc} = 540 nm; λ_{read} = 590 nm). Fluorescence data were normalized, data were fitted using GraphPad Prism Software and IC_{50} was calculated by non-linear regression.

ACKNOWLEDGEMENTS

The authors thank Mathilde Chaboud and Dr. Philippe Goldner for their help in the determination of singlet oxygen quantum yield. This work was financially supported by an ERC Consolidator Grant PhotoMedMet to G.G. (GA 681679) and by a Qlife prématuration funding (G.G. and R.V.).

SUPPORTING INFORMATION

Scheme of synthesis (S1). ^{1}H and ^{13}C NMR spectra (Fig. S1-S14). ESI-HRMS spectra (Fig. S15-S21) Comparative representation of complexes 1-9 phototoxicity upon irradiation at 480 nm for 10 min in HeLa and RPE-1 cells (Fig. S22).

REFERENCES

(1) Dolmans, D. E. J. G. J.; Fukumura, D.; Jain, R. K. Photodynamic Therapy for Cancer. *Nat. Rev. Cancer* **2003**, *3* (5), 380–387. https://doi.org/10.1038/nrc1071.

(2) Heinemann, F.; Karges, J.; Gasser, G. Critical Overview of the Use of Ru(II) Polypyridyl Complexes as Photosensitizers in One-Photon and Two-Photon Photodynamic Therapy. *Acc. Chem. Res.* **2017**, *50* (11), 2727–2736. https://doi.org/10.1021/acs.accounts.7b00180.

(3) McFarland, S. A.; Mandel, A.; Dumoulin-White, R.; Gasser, G. Metal-Based Photosensitizers for Photodynamic Therapy: The Future of Multimodal Oncology? *Curr. Opin. Chem. Biol.* **2020**, *56*, 23–27. https://doi.org/10.1016/j.cbpa.2019.10.004.

(4) Monro, S.; Colón, K. L.; Yin, H.; Roque, J.; Konda, P.; Gujar, S.; Thummel, R. P.; Lilge, L.; Cameron, C. G.; McFarland, S. A. Transition Metal Complexes and Photodynamic Therapy from a Tumor-Centered Approach: Challenges, Opportunities, and Highlights from the Development of TLD1433. *Chem. Rev.* **2019**, *119* (2), 797–828. https://doi.org/10.1021/acs.chemrev.8b00211.

(5) Karges, J.; Heinemann, F.; Jakubaszek, M.; Maschietto, F.; Subecz, C.; Dotou, M.; Vinck, R.; Blacque, O.; Tharaud, M.; Goud, B.; Viñuelas-Zahinos, E.; Spingler, B.; Ciofini, I.; Gasser, G. Rationally Designed Long-Wavelength Absorbing Ru(II) Polypyridyl Complexes as Photosensitizers for Photodynamic Therapy. *J. Am. Chem. Soc.* **2020**, *142* (14), 6578–6587. https://doi.org/10.1021/jacs.9b13620.

(6) Knoll, J. D.; Turro, C. Control and Utilization of Ruthenium and Rhodium Metal Complex Excited States for Photoactivated Cancer Therapy. *Coord. Chem. Rev.* **2015**, *282–283*, 110–126. https://doi.org/10.1016/j.ccr.2014.05.018.

(7) Mari, C.; Pierroz, V.; Ferrari, S.; Gasser, G. Combination of Ru(II) Complexes and Light: New Frontiers in Cancer Therapy. *Chem. Sci.* **2015**, *6* (5), 2660–2686. https://doi.org/10.1039/C4SC03759F.

(8) Zeng, L.; Gupta, P.; Chen, Y.; Wang, E.; Ji, L.; Chao, H.; Chen, Z.-S. The Development of Anticancer Ruthenium(II) Complexes: From Single Molecule Compounds to Nanomaterials. *Chem. Soc. Rev.* **2017**, *46* (19), 5771–5804. https://doi.org/10.1039/c7cs00195a.

(9) Poynton, F. E.; Bright, S. A.; Blasco, S.; Williams, D. C.; Kelly, J. M.; Gunnlaugsson, T. The Development of Ruthenium(II) Polypyridyl Complexes and Conjugates for in Vitro Cellular and in Vivo Applications. *Chem. Soc. Rev.* **2017**, *46* (24), 7706–7756. https://doi.org/10.1039/C7CS00680B.

(10) McKenzie, L. K.; Bryant, H. E.; Weinstein, J. A. Transition Metal Complexes as Photosensitisers in One- and Two-Photon Photodynamic Therapy. *Coord. Chem. Rev.* **2019**, *379*, 2–29. https://doi.org/10.1016/j.ccr.2018.03.020.

(11) Banerjee, S. Polypyridyl Ruthenium(II) Complexes with Red-Shifted Absorption: New Promises in Photodynamic Therapy. *ChemBioChem* Online ahead of print: https://chemistry-europe.onlinelibrary.wiley.com/doi/pdf/10.1002/cbic.202100102. https://doi.org/10.1002/cbic.202100102.

(12) Karges, J.; Kuang, S.; Maschietto, F.; Blacque, O.; Ciofini, I.; Chao, H.; Gasser, G. Rationally Designed Ruthenium Complexes for 1- and 2-Photon Photodynamic Therapy. *Nat. Commun.* **2020**, *11* (1), 3262. https://doi.org/10.1038/s41467-020-16993-0.

(13) Karges, J.; Li, J.; Zeng, L.; Chao, H.; Gasser, G. Polymeric Encapsulation of a Ruthenium Polypyridine Complex for Tumor Targeted One- and Two-Photon Photodynamic Therapy. *ACS Appl. Mater. Interfaces* **2020**, *12* (49), 54433–54444. https://doi.org/10.1021/acsami.0c16119.

(14) Karges, J.; Kuang, S.; Ong, Y. C.; Chao, H.; Gasser, G. One- and Two-Photon Phototherapeutic Effects of RuII Polypyridine Complexes in the Hypoxic Centre of Large Multicellular Tumor Spheroids and Tumor-Bearing Mice. *Chem Eur J* **2021**, *27* (1), 362–370. https://doi.org/10.1002/chem.202003486.

(15) Roy, S.; Colombo, E.; Vinck, R.; Mari, C.; Rubbiani, R.; Patra, M.; Gasser, G. Increased Lipophilicity of Halogenated Ruthenium(II) Polypyridyl Complexes Leads to Decreased Phototoxicity in Vitro When Used as Photosensitizers for Photodynamic Therapy. *ChemBioChem* **2020**, *21* (20), 2966–2973. https://doi.org/10.1002/cbic.202000289.

(16) Gkika, K. S.; Byrne, A.; Keyes, T. E. Mitochondrial Targeted Osmium Polypyridyl Probe Shows Concentration Dependent Uptake, Localisation and Mechanism of Cell Death. *Dalton Trans.* **2019**, *48* (47), 17461–17471. https://doi.org/10.1039/C9DT02967B.

(17) Kober, E. M.; Sullivan, B. P.; Dressick, W. J.; Caspar, J. V.; Meyer, T. J. Highly Luminescent Polypyridyl Complexes of Osmium(II). *J. Am. Chem. Soc.* **1980**, *102* (24), 7383–7385. https://doi.org/10.1021/ja00544a048.

(18) Zhang, P.; Huang, H. Future Potential of Osmium Complexes as Anticancer Drug Candidates, Photosensitizers and Organelle-Targeted Probes. *Dalton Trans.* **2018**, *47* (42), 14841–14854. https://doi.org/10.1039/C8DT03432J.

(19) Zhang, P.; Wang, Y.; Qiu, K.; Zhao, Z.; Hu, R.; He, C.; Zhang, Q.; Chao, H. A NIR Phosphorescent Osmium(II) Complex as a Lysosome Tracking Reagent and Photodynamic Therapeutic Agent. *Chem. Commun.* **2017**, *53* (91), 12341–12344. https://doi.org/10.1039/C7CC07776A.

(20) Glazer, E. C. Panchromatic Osmium Complexes for Photodynamic Therapy: Solutions to Existing Problems and New Questions. *Photochem. Photobiol.* **2017**, *93* (5), 1326–1328. https://doi.org/10.1111/php.12796.

(21) Lazic, S.; Kaspler, P.; Shi, G.; Monro, S.; Sainuddin, T.; Forward, S.; Kasimova, K.; Hennigar, R.; Mandel, A.; McFarland, S.; Lilge, L. Novel Osmium-Based Coordination Complexes as Photosensitizers for Panchromatic Photodynamic Therapy. *Photochem. Photobiol.* **2017**, *93* (5), 1248–1258. https://doi.org/10.1111/php.12767.

(22) Sun, Y.; Joyce, L. E.; Dickson, N. M.; Turro, C. DNA Photocleavage by an Osmium(Ii) Complex in the PDT Window. *Chem. Commun.* **2010**, *46* (36), 6759–6761. https://doi.org/10.1039/c0cc02571b.

(23) Balasubramanian, K. K.; Cammarata, V.; Wu, Q. Langmuir-Schaefer Films: Head Group Influence on Orientation of Substituted Styryl Bipyridines. *Langmuir* **1995**, *11* (5), 1658–1665. https://doi.org/10.1021/la00005a039.

(24) Storrier, G. D.; Colbran, S. B. Syntheses, Electrochemistry and Electrodeposition of Ruthenium(II) Complexes of 4,4′-Bis(4-Anilinovinyl)-2,2′-Bipyridine. *Polyhedron* **1997**, *16* (16), 2705–2710. https://doi.org/10.1016/S0277-5387(97)00049-1.

(25) Holmlin, R. E.; Yao, J. A.; Barton, J. K. Dipyridophenazine Complexes of Os(II) as Red-Emitting DNA Probes: Synthesis, Characterization, and Photophysical Properties. *Inorg. Chem.* **1999**, *38* (1), 174–189. https://doi.org/10.1021/ic9808955.

(26) Rautio, J.; Kumpulainen, H.; Heimbach, T.; Oliyai, R.; Oh, D.; Järvinen, T.; Savolainen, J. Prodrugs: Design and Clinical Applications. *Nat. Rev. Drug Discov.* **2008**, *7* (3), 255–270. https://doi.org/10.1038/nrd2468.

(27) American Society for Pharmacology and Experimental Therapeutics. *Drug Metabolism and Disposition*; American Society for Pharmacology and Experimental Therapeutics.: Bethesda, Md., 1997.

(28) Hansch, Corwin.; Leo, A.; Taft, R. W. A Survey of Hammett Substituent Constants and Resonance and Field Parameters. *Chem. Rev.* **1991**, *91* (2), 165–195. https://doi.org/10.1021/cr00002a004.
(29) McCusker, C. E.; McCusker, J. K. Synthesis and Spectroscopic Characterization of CN-Substituted Bipyridyl Complexes of Ru(II). *Inorg. Chem.* **2011**, *50* (5), 1656–1669. https://doi.org/10.1021/ic102085b.
(30) Bronner, C.; Wenger, O. S. Long-Range Proton-Coupled Electron Transfer in Phenol–Ru(2,2′-Bipyrazine)32+ Dyads. *Phys. Chem. Chem. Phys.* **2014**, *16* (8), 3617–3622. https://doi.org/10.1039/C3CP55071K.
(31) Hamann, T. W.; Gstrein, F.; Brunschwig, B. S.; Lewis, N. S. Measurement of the Free-Energy Dependence of Interfacial Charge-Transfer Rate Constants Using ZnO/H2O Semiconductor/Liquid Contacts. *J. Am. Chem. Soc.* **2005**, *127* (21), 7815–7824. https://doi.org/10.1021/ja0436188.
(32) Aranyos, V.; Hjelm, J.; Hagfeldt, A.; Grennberg, H. Electropolymerisable Bipyridine Ruthenium(II) Complexes. Synthesis and Electrochemical Characterisation of 4-(3-Methoxystyryl)- and 4,4′-Di(3-Methoxystyryl)-2,2′-Bipyridine Ruthenium Complexes. *J. Chem. Soc. Dalton Trans.* **2001**, No. 8, 1319–1325. https://doi.org/10.1039/B008697P.
(33) Sinha, S.; Mandal, S.; Gupta, P. Cyclometalated Iridium(III) Complexes of (Aryl)Ethenyl Functionalized 2,2′-Bipyridine: Synthesis, Photophysical Properties and Trans–Cis Isomerization Behavior. *RSC Adv.* **2015**, *5* (120), 99529–99539. https://doi.org/10.1039/C5RA16214A.
(34) Gajardo, F.; Barrera, M.; Vargas, R.; Crivelli, I.; Loeb, B. Influence of the Nature of the Absorption Band on the Potential Performance of High Molar Extinction Coefficient Ruthenium(II) Polypyridinic Complexes As Dyes for Sensitized Solar Cells. *Inorg. Chem.* **2011**, *50* (13), 5910–5924. https://doi.org/10.1021/ic1020862.
(35) Kochevar, I. E.; Redmond, R. W. Photosensitized Production of Singlet Oxygen. *Methods Enzymol.* **2000**, *319*, 20–28. https://doi.org/10.1016/s0076-6879(00)19004-4.
(36) Garcìa-Fresnadillo, D.; Georgiadou, Y.; Orellana, G.; Braun, A. M.; Oliveros, E. Singlet-Oxygen (1Δg) Production by Ruthenium(II) Complexes Containing Polyazaheterocyclic Ligands in Methanol and in Water. *Helv. Chim. Acta* **1996**, *79* (4), 1222–1238. https://doi.org/10.1002/hlca.19960790428.